ELSEVIER

Spectrochimica Acta Part B 63 (2008) 312–323

SPECTROCHIMICA ACTA PART B

www.elsevier.com/locate/sab

Effect of target composition on the emission enhancement observed in Double-Pulse Laser-Induced Breakdown Spectroscopy ☆

G. Cristoforetti *, S. Legnaioli, V. Palleschi, A. Salvetti, E. Tognoni

Applied Laser Spectroscopy Laboratory, Institute for Chemical–Physical Processes Research Area of National Research Council, Via G. Moruzzi, 1, 56124 Pisa, Italy

Received 11 January 2007; accepted 10 November 2007
Available online 17 November 2007

Abstract

The effect of the matrix composition on the emission enhancement observed in Double-Pulse (DP) Laser-Induced Breakdown Spectroscopy (LIBS) was studied for several pure metal targets (Al, Au, Co, Cu, Fe, Mn, Mo, Ni, Pb, Pt, Si and W). The measurements were performed in air by using a dual-pulse Nd:YAG ns laser emitting 60mJ pulses at 1064nm wavelength. The measurement of the emission enhancement for neutral and ionic lines of all the samples showed a wide range of results. Very low enhancement was observed in Pb, Ni and Mn while the highest values of enhancement were obtained in Cu, Al and Au. The space-averaged thermodynamic parameters of the induced plasmas in DP and in SP LIBS were calculated and the enhancement of ablated atomized mass in DP case was spectroscopically estimated in all the targets. A correlation seems to exist between the ablated atomized mass enhancement and the plasma temperature increase in the DP configuration. An attempt was made to correlate the increase of these two quantities with the melting point and heat, boiling point and heat, reflectivity and ionization energy of the metal. No evident correlation was found. At the opposite, a correlation was observed between the ablated atomized mass enhancement and the thermal diffusivity of the metal.

A simple picture is proposed to explain the experimental findings. It is hypothesized that different mass ablation mechanisms prevail depending on the experimental configuration. It may be expected that in the SP case mass ablation is dominated by vaporization, while in the DP case it is dominated by phase explosion and/or melt expulsion.

Keywords: Laser-Induced Breakdown Spectroscopy; Double-Pulse; Metal; Matrix composition

1. Introduction

Laser-Induced Breakdown Spectroscopy (LIBS) is a well-known analytical technique, studied since the eighties, for determining the chemical elementary composition of solid, liquid, gaseous and aerosol samples [1]. In the last decade, a variation of the traditional LIBS technique, making use of two laser pulses separated by a suitable temporal delay, was introduced [2]. The interest in this technique, called Double-Pulse LIBS, rises from the observed improvement in the limits of detection and in the reproducibility of the measurements. In particular, in DP LIBS the intensity of the plasma emission lines can be greatly enhanced, up to factors approaching near a hundred in the best cases.

Many works have been dedicated to DP LIBS, with the aim of both establishing the optimal experimental configuration to be used in different applications and of understanding the physical mechanisms, still not clear, leading to the observed emission enhancement. The effect of experimental parameters such as energy, duration and wavelength of the two laser pulses, acquisition gate, temporal inter-pulse delay, etc. has been investigated. Works have been published on DP LIBS experiments using combinations of fs and ns lasers [3].

In this paper, only the ns–ns DP combination will be discussed, in view of the easier use in practical applications

☆ This article is published in a special honor issue dedicated to Jim Winefordner on the occasion of his retirement, in recognition of his outstanding accomplishments in analytical atomic and molecular spectroscopy.

* Corresponding author. Tel.:+39 050 3152222; fax: +39 050 3152230.
E-mail address: gabriele@ipcf.cnr.it (G. Cristoforetti).

0584-8547/$ - see front matter © 2007 Elsevier B.V. All rights reserved.
doi:10.1016/j.sab.2007.11.006

such as in situ analyses [4]. The results and discussion don't apply to the case where short pulses are used, because of the large difference of the physical processes occurring in the different experimental configurations.

A useful information, for the LIBS-user, and even more interesting for the theorist, is the knowledge of the cases (i.e. type of matrices and characteristics of emission lines) where the DP LIBS is more effective with respect to the SP configuration.

Many DP experiments have been described in the literature, differing from the matrices of the target and from the experimental configurations, showing very different emission enhancements. Unluckily, the variety of setups used makes it very hard comparing these results and composing a well-defined theoretical framework. In fact, besides the different experimental parameters (laser timing and energies, laser-to-sample distance, etc.) that can be used, the observed emission enhancement is also strongly dependent on the collecting optics geometry [5].

Among the different DP configurations used, the orthogonal re-heating configuration is probably the easier to interpret. The relatively small enhancement observed in the emission intensity can be explained by a simple re-heating, due the absorption of the second laser pulse by the plasma produced by the first laser pulse. Here, the attention will be focused on the collinear and the orthogonal pre-pulse laser beams configurations, whose enhancement mechanism has not been recognized yet. Recent works [6] suggested that the mechanisms involved in the signal enhancement in these two DP LIBS configurations are similar, originating from reduced plasma shielding. In these cases, some important key points can be summarized.

It has been found that the signal enhancement is associated to higher mass removal from the target [7,8] (corresponding to higher atomized mass), and is often accompanied by higher plasma temperature [8–10] (with respect to a single laser pulse with equal total energy). The temperature increase is typically of the order of 1000–2000K.

In the hypothesis of a Boltzmann distribution of the atomic levels population, higher temperature produces a stronger enhancement of the lines coming from higher energy levels, as observed in Refs. [11,12]. Note, however, that the increase in atomized mass is, in general, the dominant effect, since signal enhancements in DP LIBS configuration were observed even in conditions leading to a *decrease* of the plasma temperature [4,13].

On the other hand, the stronger mass atomization reflects with the same weight in a generalized enhancement of all the emission lines and both the ionization states. It has been reported that the mass removed from the target in DP case is 3–30 times higher than in SP case with the same total energy [7,14], depending on the composition of the target and on the experimental parameters used.

It is worth also remembering that, in most of the DP experiments [15,16] a substantial reduction of the plasma electron density is observed, if compared to that produced by a single pulse with equal total energy. An exception to this trend is observed for long acquisition times [17], due to slower plasma evolution in DP plasmas. Bearing in mind the Saha equation[1], which in LTE plasmas governs the equilibrium between atoms and ions, at a given temperature the decrease of electron density reflects in the increase of ions density and then in the preferential enhancement of ionic emission lines, as experimentally found [11].

Both the thermodynamic parameters of the plasma and the amount of the mass removed from the sample are affected by the laser pulse energies [12,18] and by the temporal delay between the pulses [7] as well as by the starting buffer gas pressure and composition [19]. In fact, all the four parameters affect the laser–plasma–target coupling. Hence, an optimization of the experimental conditions is necessary for maximizing the emission from the plasma (which corresponds, in practice, to maximize the plasma temperature and the mass ablation efficiency). However, as observed in the literature, even in the optimized conditions, the obtained enhancement still depends predominantly on the target composition, going from scarce signal improvements for soils samples [20] to high enhancements for aluminum targets [12].

It is then clear that individuating the target matrices for which the DP LIBS technique is more effective is important not only for application purposes but also for getting a deeper insight on the physical mechanisms involved in the DP laser ablation.

Up to now, to our knowledge, very few works have been devoted to the analysis of different target matrices in DP LIBS configuration; moreover, the obtained results did not allow to identify the most determinant property of the material in causing the emission enhancement. Stratis et al. [21] analyzed several metal targets, with significantly different thermal properties, in the orthogonal pre-pulse DP configuration. Maximum intensity enhancement ranged from 6 for steel up to 33 for copper. No evident correlation between the magnitude of the enhancement and the melting point or the thermal conductivity of the target was found. In a recent detailed work, Gautier et al. [13] analyzed the effectiveness of the DP LIBS in the collinear configuration for different materials (aluminum, synthetic glass, steel, rocks) separating the contribution of temperature and ablated mass increase. Their results suggested that the intensity enhancement tends to be higher for the matrices originating a cooler SP plasma.

In this paper, the attention is focused on several metal and semiconductor targets characterized by significantly different thermal, electronic and optical properties. Other materials such as insulators and polymers have not been considered because of their different ablation mechanism with respect to metals. In fact, in metals the product $K=\alpha^2\lambda\tau$ [22,23], which corresponds to the square of the ratio between the heat diffusion length $\sqrt{\lambda\tau}$

[1] Here, it should be noted that in typical LIBS plasmas the electron density n_e is mostly produced by the ionization of ambient air atoms. This occurs because the ambient air atoms are predominant in number in the plasma. Then, considering the Saha equation for a metal atom, $n_e \gg n_{ions}$ where n_e and n_{ion} are almost independent. This means that, if the temperature does not change too much, a growth of n_e implies a decrease of the metal ion population and vice versa.

(where λ and τ are the thermal diffusivity and the laser pulse length) and the optical skin depth α^{-1} (where α is the optical absorption coefficient) is much greater than 1, indicating that the heating is a surface process and the heat distribution under the target surface is mainly determined by the thermal diffusion. On the opposite in the insulators $K \ll 1$, i.e. the heating regime is volumetric and the heat distribution is mainly determined by the laser absorption length.

2. Experimental setup

The measurements were performed using a dual-pulse mobile LIBS instrument (MODI — MObile Dual-Pulse Instrument) produced by Marwan Technology s.r.l. (Italy) in collaboration with our laboratory [4]. The instrument incorporates a dual-pulse laser, constituted by a double-rod resonator pumped by a single flashlamp, emitting two collinear laser pulses of about 10ns duration (FWHM) with energy per pulse variable between 50 and 150mJ at a maximum repetition rate of 10Hz. The inter-pulse delay can be set from 0 (single pulse) to 60μs. The laser pulse energies can be varied independently for the two beams.

The metal targets, with the surface perpendicular to the laser beams, were placed inside the MODI experimental chamber, on a motorized table for positioning at the optimal lens-to-sample distance. The sample surface was previously polished with micro-fine sandpaper and cleaned with alcohol, to increase the reproducibility of measurements.

The two beams were focused on the target surface by means of a 100mm focal length lens; the lens-to-sample distance was set 5mm less than the lens focal length for all the targets, in order to avoid the air breakdown in front of the target and to improve the stability of the plasma. The reproducibility of the lens-to-sample distance was guaranteed by means of a triangulation system formed by two non-collinear He–Ne lasers beams, crossing on the surface at the chosen focusing distance. The crossing position of the two beams was observed by a digital optical microscope.

In order to reduce the uncertainty of the observed DP signal enhancement due to the different spatial emissivity distribution for different matrices, the space-integrated LIBS signal was collected through an optical quartz fiber (diameter = 600 μm, N. A. = 0.22), placed at 45° with respect to the laser beam axis at a 3cm distance from the target surface. The optical signal was then sent to the MODI Echelle spectrometer ($\lambda / \Delta\lambda = 7500$) coupled with an intensified CCD camera, which provided for each acquisition a full spectrum in the range between 200 and 900nm.

All the acquired spectra were rescaled by the curve of spectral efficiency of the detection system, which was calculated by means of a deuterium–halogen calibrated light source by Avantes Inc.

All the experimental operations, including sample movement, settings of the laser (energy of the beams, delay between the pulses, repetition rate) and setting of the spectral acquisition parameters (number of spectra averaged, acquisition delay, CCD measurement gate and gain), were controlled by the MODI integrated computer.

The delay between the laser pulses was changed between 0, corresponding to single pulse, and 50μs. In all the measurements, an acquisition delay time of 1μs with respect to the second laser pulse was chosen in order to allow the decay of continuum, due to the Bremsstrahlung radiation and free-bound electronic recombination. An acquisition gate of 1μs was also chosen, which guaranteed well visible emission signals in all the different experimental conditions analyzed, but still allowing a meaningful calculation of the spatially integrated thermodynamic parameters of the plasma.

The energy of both the laser pulses was set to 60mJ, corresponding to an irradiance on the target of $\sim 10^{10}$W cm^{-2}.

In order to reduce the spectral fluctuations, a series of 40 pairs of laser pulses was averaged for each measurement, at a repetition rate of 2Hz.

3. Results

The aim of this work was correlating the effectiveness of DP LIBS with the thermal and optical properties of the samples.

The samples used in the analyses are almost pure targets (>99% in weight) of Al, Au, Co, Cu, Fe, Mn, Mo, Ni, Pb, Pt, Si and W. All of them, except Si, are metals and undergo a surface heating process ($K \gg 1$). Silicon has been analyzed even if it has a border-line behavior: in fact in the solid state the heating is volumetric ($K \ll 1$) since the absorption layer of the laser at 1064nm is quite high (around 200μm). However, at the opposite, in the molten state it behaves like a metal having a reflectivity higher than 90%, a laser absorption layer of few microns and showing a heating surface process.

All the measurements presented here are space-integrated and time-resolved ($\Delta t_{delay} = \Delta t_{gate} = 1$ μs); then, the calculated temperature and electron density values are space-averaged and the atomized mass estimation is obtained in the approximation of homogeneous plasma.

Hereafter, the enhancements of lines intensity (R_I) and ablated atomized mass (R_M) and the temperature increase (ΔT) in Double-Pulse configuration (DP, with laser pulses energies 60 mJ + 60mJ) with respect to the Single-Pulse configurations of

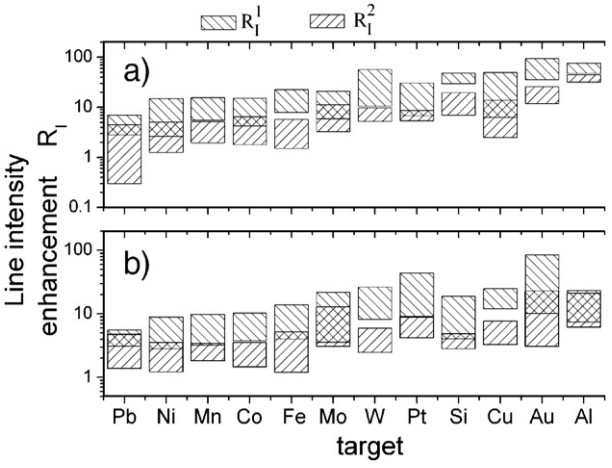

Fig. 1. Ranges of enhancements R_I^1 and R_I^2 for a) ionic lines and b) neutral lines observed in the spectral range 200–900 nm at an inter-pulse delay of 1 μs.

energy 60mJ (SP) and 120mJ (SP2, corresponding to DP at zero inter-pulse delay) will be indicated with superscripts 1 and 2, respectively.

3.1. Line intensities enhancement

For each matrix, both enhancements R_I^1 and R_I^2 are in general different for lines originated by different atomic levels (in particular depending on the energy of the upper level) and depend on the temporal delay between the laser pulses. However, the maximum enhancement is usually obtained for an inter-pulse delay around a few μs.

As an example, in Fig. 1 the ranges of enhancements R_I^1 and R_I^2 are reported for an inter-pulse delay of 1μs. In the figure all the lines visible in the 200–900nm spectrum are considered and no systematic analysis of self-absorption of the lines has been done. At a first glance, the DP LIBS enhancements are largely different for the different matrices, going from metals with modest benefits such as Pb and Ni up to metals with strong enhancements, such as Cu, Au and Al. Larger enhancements are obtained for ionic lines ($2.6<R_I^1<93$ and $0.3<R_I^2<44$) with respect to the atomic lines ($2.8<R_I^1<84$ and $1.2<R_I^2<23$). The range of enhancements spanned by the ionic lines is also larger than for atomic lines. Moreover, the maximum line enhancement calculated is just a lower limit since many lines are detected in the DP spectra and not in SP and SP2 spectra. This especially apply to ionic lines.

As reminded above, the enhancement observed in Fig. 1 is caused on one side by change of thermodynamic parameters in SP, SP2 and DP plasmas and on the other side by the increase of the atomized mass in the plasma. In order to separate these causes, we calculated the temperature and electron density of plasmas in SP, SP2 and DP cases.

3.2. Plasma electron density

The spatially averaged electron density was calculated by measuring the Stark broadening of the Balmer H_α line, according to the formula [24] $n_e(cm^{-3})=8.02\cdot 10^{12}(\Delta\lambda_{1/2}/\alpha_{1/2})^{3/2}$ where $\Delta\lambda_{1/2}$ is the FWHM in Angstrom and $\alpha_{1/2}$ is a coefficient, weakly depending on electron density and temperature, tabulated by Griem [25]. Hydrogen emission is always present in the LIBS spectra taken in ambient air, because of the water vapor due to the natural humidity of the air. The use of the H_α line for the measurement of the electron density has the definite advantage of providing a result which is not affected by self-absorption, unless the sample itself would contain high levels of hydrogen. Moreover, the linear Stark effect acting on hydrogen lines produces a large broadening which results in a smaller uncertainty with respect to the measurement made by using lines emitted by other elements.

In Fig. 2a, for instance, the electron density calculated for several targets and inter-pulse delays is reported. For all the matrices (included those not plotted), whatever is the emission enhancement observed, the electron density in the DP plasmas is always lower than that in the SP2 case, in accordance to what observed in previous works [15,16].

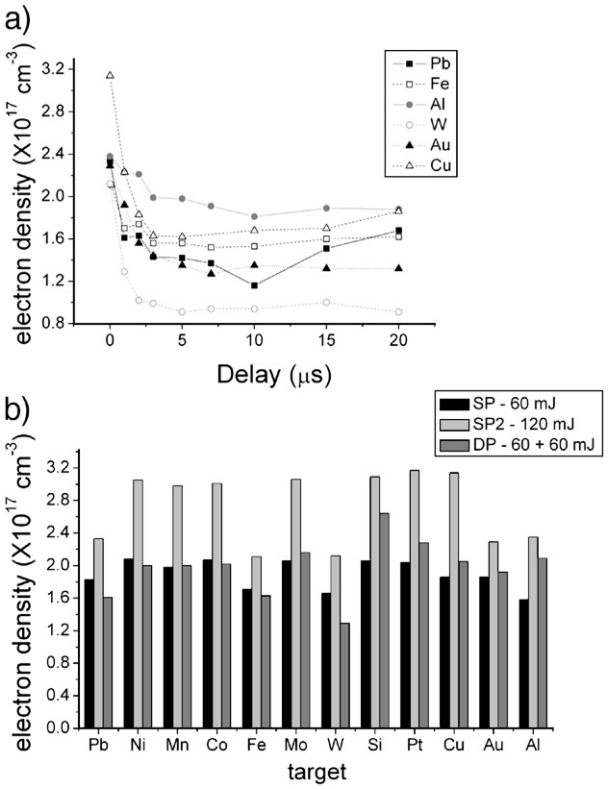

Fig. 2. a) Electron density calculated for several matrices at different inter-pulse delays; the uncertainty on n_e is of the order of 10%; b) electron density calculated for all the matrices at an inter-pulse delay of 1 μs.

In Fig. 2b the electron density calculated for all the targets at an inter-pulse delay of 1μs is reported.

While the electron density in the SP2 case is the highest among the three configurations, the SP and the DP cases evidence electron densities generally comparable. However, the electron density in the matrices characterized by more pronounced enhancements seems to increase from SP to DP case, though the uncertainty of n_e values (mainly due the laser–matter interaction reproducibility) is often comparable with the variations.

3.3. Plasma temperature

The spatially averaged plasma temperature has been also calculated, in the framework of the Local Thermal Equilibrium (LTE) approximation, using the Saha–Boltzmann plot method, as described in Ref. [26]. This method consists in a generalization of the Boltzmann plot which takes into account both neutral and ionized lines, through the use of the Saha equation and of the values of plasma electron density previously calculated. The advantage of using such method is the larger range obtained in the upper energies of the lines plotted (in many cases $\Delta E\sim 8$–10eV) which leads to a substantial reduction of the uncertainty of the calculated temperature $\left(\frac{\Delta T}{T}\propto\frac{T}{\Delta E}\right)$.

In this way, the precision on determination of the absolute value of the temperature is of the order of 5–10%, depending on

Table 1
Emission lines used for calculating the plasma temperature in the different matrices

	Species	λ (nm)	E_k (cm^{-1})	E_i (cm^{-1})	A_{ki} (10^8 s^{-1})
Aluminum	Al I	305.0	61,844	29,067	0.32
	Al I	305.5	61,748	29,020	0.45
	Al I	305.7	61,844	29,143	0.75
	Al II	281.6	95,351	59,852	3.83
	Al II	358.6	123,420	95,549	5.39 [a]
	Al II	466.4	106,920	85,481	0.53
Cobalt	Co I	339.5	34,134	4690	0.29
	Co I	384.2	33,463	7442	0.13
	Co I	384.5	33,440	7442	0.46
	Co I	387.3	29,295	3483	0.12
	Co I	399.8	33,467	8461	0.07
	Co I	409.2	31,871	7442	0.057
	Co I	411.0	32,782	8461	0.055
	Co I	411.9	32,733	8461	0.16
	Co I	412.1	31,700	7442	0.19
	Co II	266.3	47,346	9813	0.53
	Co II	281.1	45,379	9813	0.014
	Co II	283.5	45,972	10,708	0.01
	Co II	335.3	47,849	18,032	0.029
	Co II	362.1	45,379	17,772	0.026
Copper	Cu I	310.0	71,268	39,019	0.26
	Cu I	312.6	70,998	39,019	0.76
	Cu II	250.6	108,340	68,448	1.84
	Cu II	270.1	110,370	73,353	0.66
	Cu II	270.3	110,080	73,102	1.18
Gold	Au I	274.8	45,537	9161	0.48
	Au I	302.9	42,164	9161	0.08
	Au I	312.3	41,175	9161	0.19
	Au I	389.8	67,811	42,164	0.28
	Au I	448.8	67,811	45,537	0.20
	Au I	479.3	62,034	41,175	0.89
	Au II	299.0	48,014	14,582	0.015
Iron	Fe I	381.6	38,175	11,976	1.3
	Fe I	382.0	33,096	6928	0.67
	Fe I	407.2	37,521	12,969	0.76
	Fe I	426.1	42,816	19,351	0.32
	Fe I	432.6	36,079	12,969	0.5
	Fe I	440.5	35,257	12,561	0.27
	Fe II	268.5	68,001	30,764	1.4
	Fe II	278.4	62,083	26,170	0.7
	Fe II	278.5	77,862	41,968	1.0
	Fe II	300.3	46,967	13,673	0.14
Lead	Pb I	244.4	48,726	7819	0.44
	Pb I	244.6	48,687	7819	0.25
	Pb I	247.6	48,189	7819	0.38
	Pb I	257.7	49,440	10,650	0.67
	Pb II	676.0	74,459	59,449	0.74
Manganese	Mn I	325.6	48,271	17,568	0.5
	Mn I	325.8	48,318	17,637	0.97
	Mn I	326.5	47,904	17,282	0.14
	Mn I	373.2	61,211	34,423	1.0
	Mn I	460.5	59,828	38,120	0.36
	Mn I	462.7	59,617	38,009	0.36
	Mn II	253.6	67,009	27,584	0.42
Molybdenum	Mo I	407.0	41,348	16,784	0.33
	Mo I	423.3	40,367	16,748	0.32
	Mo I	481.9	42,088	21,343	0.27
	Mo I	550.6	28,924	10,768	0.36
	Mo I	557.0	28,715	10,768	0.33
	Mo I	579.2	28,715	11,454	0.06
Molybdenum	Mo I	585.8	28,924	11,858	0.028
	Mo II	242.4	65,075	23,833	0.14
	Mo II	315.3	58,197	26,488	0.66
	Mo II	332.1	55,216	25,112	0.76
Nickel	Ni I	301.2	36,601	3410	1.3
	Ni I	308.1	34,163	1713	0.09
	Ni I	478.7	48,467	27,580	0.18
	Ni I	547.7	32,982	14,729	0.095
	Ni II	233.5	56,371	13,550	0.8
	Ni II	237.5	57,081	14,996	0.66
	Ni II	243.8	54,557	13,550	0.54
	Ni II	251.1	53,365	13,550	0.58
Platinum [b]	Pd I	342.1	36,976	7755	1.68
	Pd I	344.1	40,771	11,722	2.46
	Pd I	346.1	35,451	6564	0.3
	Pd I	355.3	39,858	11,722	2.62
	Pd I	361.0	35,451	7755	0.82
	Pd II	285.5	67,299	32,278	2.8
Silicon	Si I	243.6	47,352	6299	0.47
	Si I	263.1	53,387	15,394	0.97
	Si I	298.8	39,760	6299	0.024
	Si I	390.6	40,992	15,394	0.12
	Si II	504.1	101,020	81,191	0.98
	Si II	505.6	101,020	81,251	1.2
Tungsten	W I	321.6	37,309	6219	0.26
	W I	429.5	26,230	2951	0.13
	W I	484.4	23,965	3326	0.016
	W I	488.7	26,676	6219	0.008
	W II	244.6	48,284	7420	0.41
	W II	361.4	42,298	14,634	0.11
	W II	365.8	36,165	8833	0.054
	W II	373.6	44,758	18,001	0.035

[a] The Al II 358.6 is a multiplet formed by 3 lines which are not resolved; then the A_{ki} used is an effective value calculated by using the spectroscopic parameters of these lines.
[b] In the platinum target, the temperature was calculated by using the emission lines of palladium, which is less than 1% of the matrix.

the matrix and on the lines utilized. This error, as showed in the following, can be too large for discriminating the plasma temperature variations obtained on different matrices. However, when comparing the temperature variations obtained on the same matrix in SP, SP2 and DP configurations, the uncertainty on the A_{ki} coefficients and on the apparatus efficiency curve can be neglected leading to an accuracy on temperature calculation of the order of 3–5%, coming mainly from the uncertainties on the electron density and the fitting of the line profile. Since the temperature values found for the same matrix in SP, SP2 and DP configurations differ by much more than this value, their comparison is significant.

The emission lines used for calculating the temperature in all the matrices were listed in Table 1. All lines have been carefully chosen, making use of a home-made simulation software, for avoiding the occurrence of self-absorption effects.

As observable in Fig. 3a, the trend of the temperature with the inter-pulse delay is different for the matrices plotted. While in Al and Au the temperature in DP is much higher than that obtained with coincident laser pulses, in Pb and W an evident decrease is found.

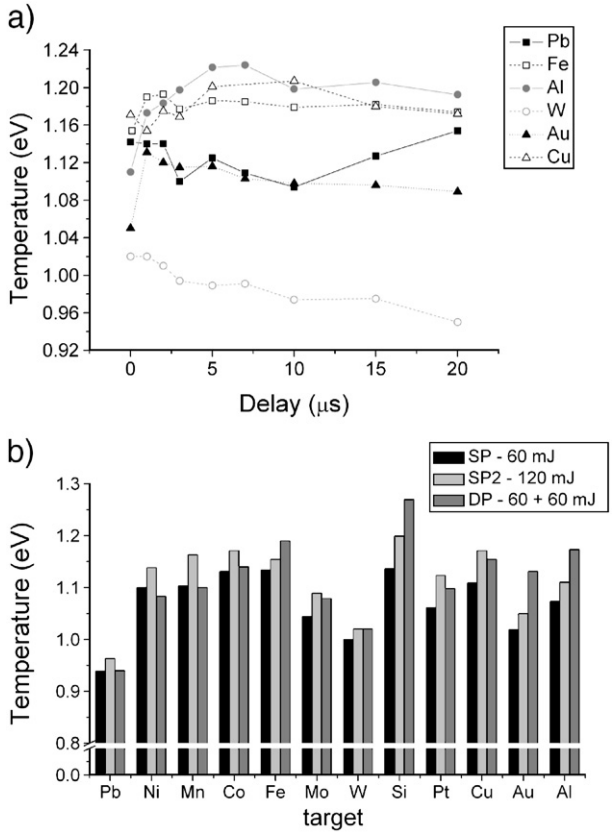

Fig. 3. a) Temperature calculated for several matrix targets at different inter-pulse delays; the uncertainty on T to be considered here is ~3–5% depending on the matrix; b) temperature calculated for the matrices at an inter-pulse delay of 1 μs.

In Fig. 3b the temperature calculated for all the targets at an inter-pulse delay of 1μs is reported. Due to the large error on the absolute value of T, all the values calculated for the different matrices are comparable within the error. On the other hand, by looking at the variations found in the different configurations, it is clear that for all the targets, as expected, the temperature of plasmas obtained in SP2 is higher than that obtained in SP. A clear relation between temperatures and enhancements is not straightforward. Nevertheless, similarly to what observed for the electron density, the temperature values obtained in DP for the targets characterized by a more pronounced signal enhancement is typically higher than in the SP case. A different behavior is generally observed in the other cases.

3.4. Plasma ablated mass

In a previous paper [12], where a collinear DP configuration was tested on an Al target, it was shown that the signal enhancement R_I^2 was dominated by the increase in ablated atomized mass. In fact, the increase of ablated atomized mass resulted $R_M^2 \sim 7$, contributing to R_I^2 by the same factor. The temperature increase ΔT, instead, contributed to R_I^2 by a factor 0.94–1.2 for neutral lines and 2.3–3 for ionic lines. Moreover, since the former factor affects all the lines in the same way, it is important to estimate the increase of the atomized mass in the plasma, in order to make a comparison among the different targets.

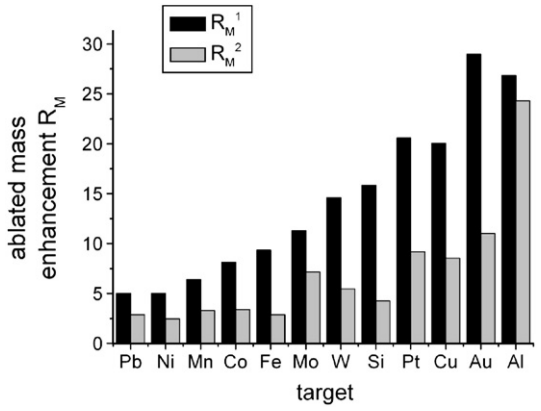

Fig. 4. Ablated atomized mass enhancements R_M^1 and R_M^2 for all the targets. Measurements are done at an inter-pulse delay of 1 μs. The uncertainty is ~25–30%.

However, finding the increase of mass in the plasma is not easy. A direct measurement of crater dimensions would be a useful information but it can be not suitable for our purpose, because of the difficulty of measuring the real ablated mass (often, the volume of the crater is similar to that of the rim around the hole [12]). Moreover, the measure of crater dimension does not discriminate between the mass atomized and that ejected (and lost) in clusters. An estimation of the atomized mass increase in the plasma can be obtained via spectroscopic measurements, though it might be affected by the uncertainties in the determination on the thermodynamic parameters and by the geometry of signal collection in the experimental setup.

In this work, the experimental setup has been specifically designed for reducing these sources of uncertainty. Assuming the Local Thermal Equilibrium in the plasma, the lines emitted by a species s can be represented in a Boltzmann plot, according to the linear relation $y=mx+q_s$. Such quantities are defined as $y=\ln(I_{ki} / g_k A_{ki})$, $x=E_k$, $m=-1/k_B T$ and $q_s=\ln(N_s F / U_s(T))$, where I_{ki} and A_{ki} are the integrated intensity and the transition probability of the line, E_k and g_k are the energy and the degeneracy of the atomic upper line of the transition, k_B is the

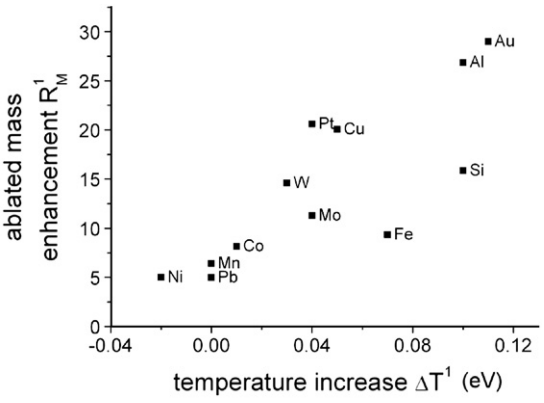

Fig. 5. Ablated atomized mass enhancement vs. temperature increase of DP LIBS with respect to SP. Measurements are done at an inter-pulse delay of 1 μs.

Boltzmann constant, T and $U_s(T)$ are the plasma temperature and the partition function at such temperature, F is an experimental factor and N_s is the number of atoms of the species present in the plasma.

It is then assumed that parameter F is the same in DP, SP and SP2. This hypothesis is valid if, in all the LIBS configurations [5], the emission from all the regions of the plasma is collected in the spectrometer without any spatial selection; the choice of optical fiber detection in our experimental setup responds to this requirement.

At this point, assuming that the plasma temperature can be calculated, the ablated mass enhancement R_M can be estimated from the relation

$$R_M^{1,2} = \frac{U_I(T_{DP})\exp\left(q_I^{DP}\right) + U_{II}(T_{DP})\exp\left(q_{II}^{DP}\right)}{U_I\left(T_{SP,SP2}\right)\exp\left(q_I^{SP,SP2}\right) + U_{II}\left(T_{SP,SP2}\right)\exp\left(q_{II}^{SP,SP2}\right)}$$

where the subscripts I and II refer to the atomic and ionic species and the q-parameters are determined by the fitting of the emission lines plotted in the Boltzmann plane.

It is well-known among the spectrochemists that the calculation of the emitter density by a spectroscopic approach may be largely inaccurate and then often useless. However, it can be easily shown that the uncertainty of the mass ratio R_M is strongly reduced because of its substantial independence from the transition probabilities A_{ki} of the lines and from the spectral efficiency of the detecting apparatus. So, taking into account the uncertainties of the line intensity (~5% if self-absorption is not present), of the electron density (~10%) and of the partition functions (depending on the uncertainty on the temperature T, which is of the order of 5–10%), a resulting uncertainty of the mass ratio R_M of about 25–30% can be calculated.

The obtained mass enhancements in the plasma are plotted in Fig. 4. By comparison of the data showed in the last two sections, a relation seems to exist between the plasma temperature increase and the ablated mass enhancement, as evident in Fig. 5, despite the uncertainty on the ΔT value. This result would imply that when the DP LIBS is most effective in increasing the ablated atomized mass it also produces a substantial increase of the plasma temperature and vice versa.

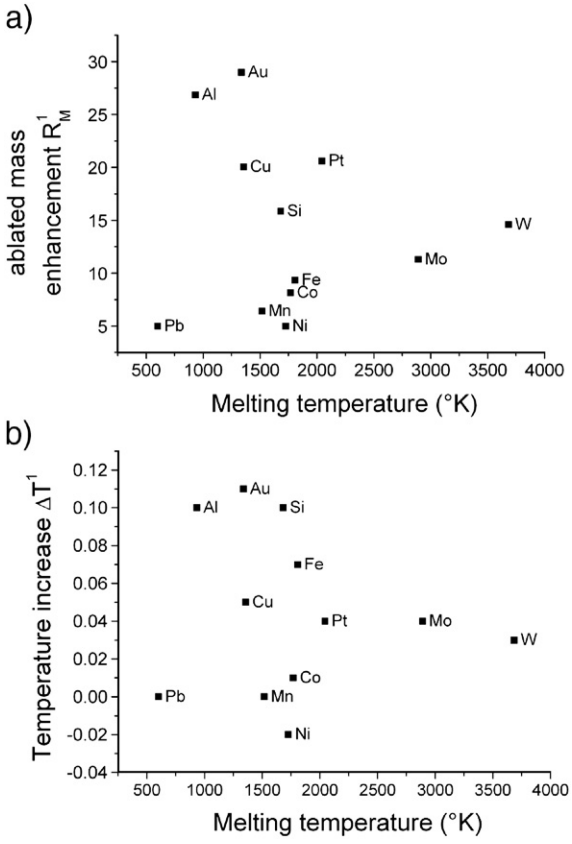

Fig. 6. a) Ablated mass enhancement R_M^1 and b) temperature increase ΔT^1 in DP with respect to SP configuration vs. melting temperature of the metal.

3.5. Enhancement vs. target properties

The subsequent step in this work was the investigation on possible relations between the target physical properties and the observed enhancement.

Table 2
Thermal and electronic properties of the targets

Matrix	T_m (°K)	T_b (°K)	Ev heat (kJ/mol)	E_{ion} (kJ/mol)	R	λ ($cm^2\ s^{-1}$)	λ_m ($cm^2\ s^{-1}$)	ΔT^1 (eV)	R_M^1
Pb	601	2024	177.7	715.6	0.84	0.218	0.110	0	5
Ni	1726	3193	370.4	736.7	0.74	0.232	0.10	−0.02	5
Mn	1517	2333	226.0	717.4		0.024	–	0	6.4
Co	1768	3373	376.5	758.4		0.268	0.06	0.01	8.1
Fe	1808	3023	349.6	759.3		0.130	0.07	0.07	9.3
Mo	2890	4923	598.0	684.9	0.57	0.540	0.143	0.04	11.3
W	3683	5773	824	770	0.58	0.689	0.18	0.03	14.6
Si	1683	3553	384	786.4	0.3	0.900	0.21	0.1	15.8
Pt	2045	4443	510	870		0.279	0.265	0.04	20.6
Cu	1357	2843	300.3	745.4	0.95	1.145	0.36	0.05	20.1
Au	1338	3081	334	890.1	0.98	1.29	0.4	0.11	29
Al	934	2740	293.4	577.6	0.91	0.974	0.42	0.1	26.9

T_m — melting temperature; T_b — boiling point; Ev heat — evaporation heat; E_{ion} — 1st ionization energy; R — reflectivity at 1064 nm; λ — thermal diffusivity; λ_m — thermal diffusivity at melting point; ΔT — temperature increase; R_M — ablated mass enhancement.

Hereafter, the SP and DP configurations will be compared at a constant inter-pulse delay of 1 μs, which corresponds for most of the matrices to the highest signal enhancement. These two configurations were chosen because, in our opinion, it is more physically significant comparing the effect of the same energy laser pulse impinging on the surface in the two completely different environmental conditions (ambient air pressure in the SP and rarefied medium in the DP). In our approach, then, the first pulse is considered just as a tool for modifying the environmental conditions where the second pulse will operate, according to a model well-discussed in the literature.

In Table 2, some thermal and optical properties of the metals analyzed are listed, together with the increase of plasma temperature ΔT^1 and mass enhancement R_M^1 in DP with respect to SP for an inter-pulse delay of 1 μs.

It is well-known that thermal properties such as melting and boiling temperatures or melting and evaporation heats are strongly correlated with the molten and vaporized volume of sample [27,28] and with the breakdown threshold [29]. Nonetheless, no clear correlation was found in our experiment between these parameters and the ablated mass enhancement or temperature increase in DP LIBS, in agreement with Stratis et al. [21]. This is evident in Fig. 6, which shows the comparison of our data on DP enhancement with the melting point; similar lack of correlation was obtained for the other thermal parameters cited above.

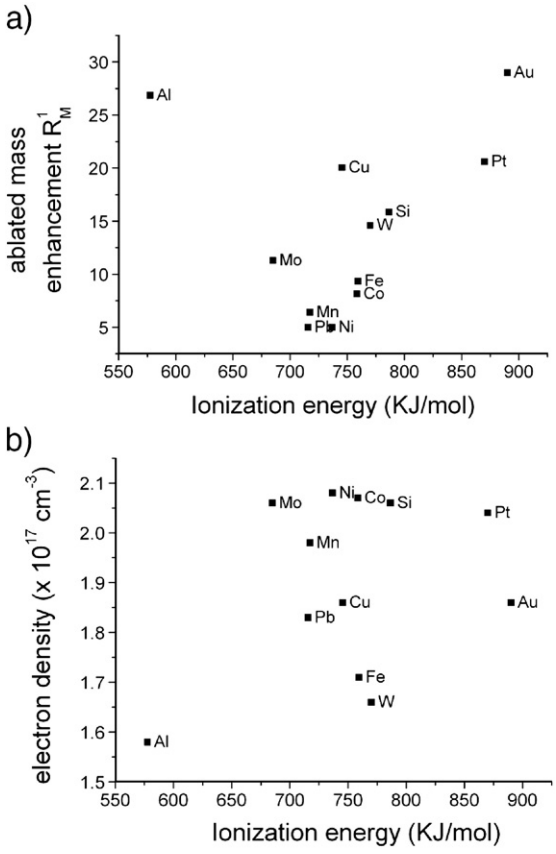

Fig. 7. a) Ablated mass enhancement R_M^1 in DP with respect to SP configuration and b) electron density in SP case vs. 1st ionization energy of the atom.

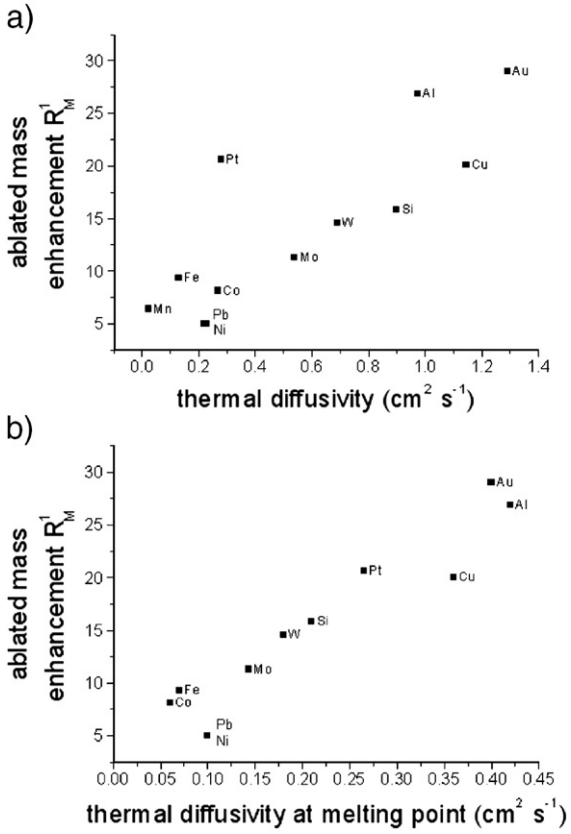

Fig. 8. Ablated mass enhancement in DP LIBS with respect to SP configuration vs. thermal diffusivity at a) ambient temperature and b) melting point.

In principle, another important parameter to consider is the 1st ionization energy of the metal, because of its hypothetical relationship with the plasma capability of shielding the laser beam. The interest is motivated by the hypothesis that a decrease of the plasma shielding in DP with respect to SP is responsible of the signal enhancement. However, a correlation between the 1st ionization energy and the mass ratio R_M^1 is not immediately evident (see Fig. 7a). Moreover, even a relation between the electron density in the plasma (strongly related to the laser shielding), and the ionization energy of the atom is not visible in the three configurations (SP, SP2 and DP), (see Fig. 7b for the SP case). Therefore, the ionization energy of the atoms seems not to be the dominant parameter in driving the DP process. This result will be more exhaustively discussed in the next paragraph.

The reflectivity of the surface at the laser wavelength (1064nm), affecting the amount of laser energy not absorbed by the target, was also considered (though it dramatically drops during the ablation process), finding no correlation with the intensity or ablated mass enhancement (the corresponding results are not shown here).

On the contrary, a definite increasing trend seems to exist between the thermal diffusivity of the target and the ablated mass enhancement, as shown in Fig. 8a. The thermal diffusivity expresses how rapidly the heat diffuses from the surface layer, where the laser impinges, towards the interior of the target. It is worth to remember that the thermal diffusivity λ is a dynamic

parameter depending on the temperature of the metal and its phase state. It means that during all the ablation process, characterized by a progressive heating of the target, its value changes, in particular dropping during the melting process. For this reason, as an indication, a plot of ablated mass enhancement vs. the thermal diffusivity at melting point was reported in Fig. 8b. It is clear that such a plot may be interesting to eventually confirm the trend observed in Fig. 8a, although it is just indicative since the temperature of the target surface reaches values, depending on the target matrix, much higher than the melting point and even higher than the boiling point.

The trend observed in Fig. 8b confirms an increasing trend between the atomized mass increase and the thermal diffusivity; moreover, since the reduction of λ with temperature is different for the metals analyzed, a reduction of the scattering of the experimental points is observed with respect to the same plot calculated using the thermal diffusivity of the target at room temperature. This consideration supports the idea that the variation of thermal diffusivity with temperature plays indeed an important role in determining the mass ablation enhancement in DP LIBS configuration.

At a first glance, such result seems to be in contrast with the results of Stratis et al. [21], who did not observe any relation between intensity enhancement and thermal conductivity K_T (which is defined in terms of the diffusivity as $K_T = \lambda \cdot c_p \cdot \rho$ where λ, c_p and ρ are the thermal diffusivity, the specific heat and the mass density). However, thermal conductivity and diffusivity are not proportional to each other in different materials. Moreover, the intensity of the lines is less significant than the atomized mass since it depends also on the atomic levels of the transition. Finally, in the Stratis work, a collecting lens was used to gather the signal, and there is no warranty that a spatial selection of the plasma emission was not present.

4. Discussion

4.1. Correlation between metal ablation efficiency in SP and enhancement in DP

As reminded above, the melting and the boiling points of the target, as well as its reflectivity, affect the amount of material vaporized during the ablation [26,27]. Qualitatively, lower values of melting and boiling points and of reflectivity are associated to higher values of ablated mass. However, the relation is not so strict, since the interplay between such parameters in the process is complex. It may happen that the ablation of a target with low reflectivity and high boiling point results in a quantity of mass removed similar to that obtained in the ablation of target with high reflectivity and low boiling point [30].

Nevertheless, as a first approximation, the absence of correlation between the ablated atomized mass enhancement and the boiling point or the reflectivity of the metal roughly suggests analogous lack of correlation between this enhancement and the amount of material removed from the target in the SP configuration. This is confirmed by considering the cases of Pb and Cu targets: both metals show large residual craters and large atomized mass in SP but this is accompanied, in the DP LIBS, by a low atomized mass enhancement for Pb and by a large enhancement for Cu.

4.2. The laser shielding hypothesis

The lack of correlation of the 1st ionization energy of the metal with the mass enhancement can cast some doubts on the importance of the laser shielding effect in causing the DP effects. At this point, it is worth to remember that the more credited interpretation of the observed DP benefits relies on the hypothesis of a lower plasma shielding of the second laser pulse, due a rarefied ambient environment, leading to a more effective laser–matter coupling. On the other hand, the validity of such a hypothesis has been tackled, discussed and substantiated with experimental results (though not analytically modelled) in a variety of papers [2,6,19,21], making it more robust than other suggested mechanisms of signal enhancement.

Iida [31] measured the amount of material removed with a single-pulse Nd:YAG laser from several metallic targets (Al, Zn, Cu, Pb, W and brass) in air at 0.1, 100 and 760torr pressures. Strong enhancement of material removal with decreasing the air pressure (and gas density) was observed, as an effect of the progressive lowering of the laser shielding. This phenomenon should be similar, in the "shielding hypothesis", to what happen when the second laser pulse strikes the target surface within a low density ambient gas bubble, created by the first laser pulse.

It is worth to note that, in Iida experiment, the mass removal enhancement at low air pressure is not correlated with the 1st ionization energy of the matrix element. Therefore, the laser shielding seems to be much more strongly affected by the ambient air composition (through the ionization energy and mass of its components) than by the ionization energy of the matrix element. This indication is confirmed in the present work by the lack of correlation found between the electron density of the plasma (whose value is mainly determined by the plasma absorption of the laser, i.e. laser shielding) in SP and the ionization energy, as visible in Fig. 7b. All these considerations suggest that the results found in this paper do not lead to an invalidation of the "shielding" interpretation, but rather to the need of a robust model of the laser shielding effect, accounting for all the experimental parameters.

Such approach has been attempted, recently, by Bleiner et al. [32] who presented a complete laser-vaporization model in a background gas. According to their model, the plasma shielding is more strongly affected by the amount of vaporized target material than by the ionization energy of the target element. For example, the authors showed that, in 1atm He conditions, the 266nm laser shielding of Al (E_{ion} = 577.6 KJ/mole) can be much lower than that of Fe (E_{ion} = 759.3 KJ/mole). This is another indication of the importance of the above cited thermal and optical properties.

4.3. The role of thermal diffusivity

In the cited work of Iida, the enhancement of ablated mass at low pressures with respect to atmospheric conditions shows a

correlation with the material thermal diffusivity. In fact, the enhancement is low for Pb, which has the lowest thermal diffusivity, and high for W, Al and Cu, characterized by higher values of such parameter. This observation fits well with the trends here plotted in Fig. 8 and strengthens the similarity between the laser ablation processes at low pressures and in the DP configuration.

In order to attempt a qualitative modelling of the correlation between the temperature increase and the ablated mass enhancement with the thermal diffusivity of the target, it is necessary to focus our attention on the role of the thermal diffusivity in the laser ablation. Such parameter determines the speed of the heat diffusion from the target surface, where the laser energy is delivered, towards the interior of the target itself. Thus, thermal diffusivity also determines the spatial distribution of the temperature in the target and the depth of the molten metal pool. For example, a metal target with low thermal diffusivity, as Mn, Fe or Co, tends to have a higher surface temperature and a thinner molten pool with respect to metals characterized by higher values of such parameter, such as Cu, Al or Au.

Explaining why this feature affects the DP benefits is not straightforward and would require an accurate knowledge of the ablation processes in the DP mode. It should be known how much the laser shielding process is affected by the matrix of the sample, and then at what extent this affects the differences in enhancement observed in DP. On the other hand it would be essential to know which is the leading mechanism of matter ablation (vaporization, phase explosion, melt splashing…) in SP and DP modes. At this level it can be said that the importance of the thermal diffusivity in determining the signal enhancement in DP LIBS configuration suggests that considering the ambient gas effects only, such as shielding and dynamical confinement, is not an adequate approach to describe the DP process. Then, the consideration of these effects, which qualitatively are thought to produce the observed increase of mass removal, must be integrated with ablation mechanisms and thermal effects in a more complete approach.

4.4. Vaporization vs. phase explosion and melt expulsion

In the framework of the model of a lower laser shielding in the DP LIBS with respect to SP, a larger amount of laser energy reaches the target in the former case, producing evidently a higher temperature of the target. In this situation a pure vaporization model of ablation hardly complies with the observation of a strong increase of material removal. In fact, in the pure vaporization model the velocity of surface recession (atoms/cm^2 s), governed by the Hertz–Knudsen equation [32], rapidly saturates with the surface temperature of the target because of the progressive increase of inverse re-condensation process. It is possible, as suggested by Colao et al. [17], that the strong heating leads the molten pool near the thermodynamic critical temperature, driving the onset of phase explosion mechanism. This would involve a shift of the phase explosion threshold towards lower irradiance levels in the DP configuration. The hypothesis of onset of phase explosion and of an increasing effect of melt splashing in the mass removal was also proposed by Mao et al. [33].

The occurrence and the characteristics of the phase explosion in (single pulse) ns laser ablation has been discussed [34–37] in recent years, since Martynyuk in the eighties first proposed this mechanism for high-fluence laser irradiated metals [38]. Nevertheless, the debate cannot be yet considered exhaustive, mainly because of the poor current knowledge of the thermal and optical properties of matter near the thermodynamic critical point. Even the qualitative characterization of laser irradiated matter near and under explosive-boiling regimes can be still considered a hard challenge. A lack of experimental measurements of phase explosion threshold on metals, especially using a IR laser, must be added to this framework.

However, what can be safely said is that the thermal diffusivity plays a fundamental role in determining the phase explosion threshold of materials and also the amount of matter ejected from the target. In first place, the high thermal diffusivity of metals, associated to their thin laser absorption layer, makes questionable the formation of a subsurface heating [36,39]. Then, it is clear that the higher the thermal diffusivity of the metal, the higher also the threshold of the boiling explosion regime, since the temperature reached by the molten pool is lower. Finally, the thermal diffusivity affects the depth of the molten metal pool; then, since the explosive boiling is a volume process, because of the contemporaneous growth of nucleation bubbles in all the volume of molten metal, the thermal diffusivity has an effect on the amount of matter ejected from the target.

Starting from these qualitative considerations, together with the hypothesis that in SP configuration a lower percentage of pulse energy reaches the target surface with respect to the DP case, a simple picture can be drawn. As a working hypothesis, we can suppose that in SP the pure vaporization mechanism is predominant (neglecting for the moment the other thermal and optical properties of the matrix). Being it a surface process, the metals with lower thermal diffusivity are favored in removing material from the target, because of the higher surface temperature reached. Moreover, in SP (where the effective irradiance is low because of the laser shielding) the threshold of the explosive-boiling regime can be more easily reached for metals with lower thermal diffusivity, which dissipate less heating in the interior of the target and for which a subsurface heating might be still possible. Both these effects concur to draw a picture where, other material properties being neglected, in SP configuration a larger ablation of matter is favored for the lower thermal diffusivity metals. On the other side, in the DP configuration, where a much larger percentage of the second pulse energy reaches the target, a different situation can occur, where all the targets probably reach the phase explosion threshold,. Here, the metals with higher thermal diffusivity are favored in expelling material for the larger depth of the molten pool, in a situation opposite to that described for SP.

Another mechanism which can be invoked for the removal of material in DP configuration, where the effective irradiance on the target is higher, is the liquid metal expulsion. In that case, whether the driving mechanism is internal to the molten pool

(explosive boiling) or external (vapor recoil pressure), the process takes place whenever a critical temperature is reached, for which the recoil and surface tension forces are equal. At that point, the extent of melting at the time when such temperature is reached determines the amount of liquid metal expelled [40]. In turn, as said above, the depth of the molten pool is determined by the thermal diffusivity of the metal. Then, in the melt expulsion mechanism, a metal with higher λ value would produce a larger volume of ablated mass.

Concluding, it is likely that the role of explosive boiling and melt expulsion grows from the SP to the DP LIBS, because of the larger effective energy reaching the target in DP configuration. The above consideration would corroborate, at least qualitatively, the trend obtained in Fig. 8. In this picture, the scattering of the experimental points seems to be, all considering, reasonable and well explainable by the experimental uncertainties together with the interplay of the other matrix properties.

5. Conclusions

The influence of the matrix composition on the Double-Pulse LIBS effectiveness has been studied for pure metal targets. The ranges of line intensity enhancement for neutral and ionic lines, obtained in Double-Pulse with respect to Single-Pulse LIBS configuration, show very different improvements going from the lowest observed in Pb, Ni and Mn up to the highest obtained in Cu, Al and Au. Moreover, an almost general larger enhancement for ionic lines with respect to atomic lines is observed. The space-averaged temperature and electron density of the induced plasmas in SP, SP2 and DP LIBS were calculated and the enhancement of ablated atomized mass in DP was spectroscopically estimated in all the targets. A decrease of electron density in DP plasmas with respect to SP2 plasmas was observed for all the inter-pulse delays used and for all the target analyzed; on the other hand, the electron density found in SP and DP cases are comparable. An attempt was made to correlate the calculated increase of plasma temperature and the ablated mass enhancement in DP case with the melting point and heat, boiling point and heat, reflectivity, as well as the ionization energy of the metal, finding no evident relation. However, a definite increasing trend was observed between the ablated mass and plasma temperature enhancements and the thermal diffusivity of the metal.

The observations are qualitatively explainable considering that the prevailing mass ablation mechanisms in the SP and in the DP cases are different, the first being dominated by vaporization, the second dominated by phase explosion and/or melt expulsion.

References

[1] E. Tognoni, V. Palleschi, M. Corsi, G. Cristoforetti, Quantitative micro-analysis by laser-induced breakdown spectroscopy: a review of the experimental approaches, Spectrochim. Acta Part B 57 (2002) 1115–1130.
[2] V.I. Babushok, F.C. DeLucia Jr, J.L. Gottfried, C.A. Munson, A.W. Miziolek, Double pulse laser ablation and plasma: laser induced breakdown spectroscopy signal enhancement, Spectrochim. Acta Part B (2006) 999–1014.
[3] J. Scaffidi, J. Pender, W. Pearman, S.R. Goode, B.W. Colston Jr., J.C. Carter, S.M. Angel, Dual-pulse laser-induced breakdown spectroscopy with combinations of femtosecond and nanosecond laser pulses, Appl. Opt. 42 (2003) 6016–6099.
[4] A. Bertolini, G. Carelli, F. Francesconi, M. Francesconi, L. Marchesini, P. Marsili, F. Sorrentino, G. Cristoforetti, S. Legnaioli, V. Palleschi, L. Pardini, A. Solvetti, Modì: a new mobile instrument for in situ double-pulse LIBS analysis, Anal. Bioanal. Chem. 385 (2006) 240–247.
[5] G. Cristoforetti, S. Legnaioli, V. Palleschi, A. Salvetti, E. Tognoni, Characterization of a collinear double pulse laser-induced plasma at several ambient gas pressure by spectrally- and time-resolved imaging, Appl. Phys. B 80 (2005) 559–568.
[6] G. Cristoforetti, S. Legnaioli, A. Salvetti, L. Pardini, V. Palleschi, E. Tognoni, Spectroscopic and shadowgraphic analysis of laser induced plasmas in the orthogonal double pulse pre-pulse configuration, Spectrochim. Acta Part B 61 (2006) 340–350.
[7] L. Caneve, F. Colao, R. Fantoni, V. Spizzichino, Laser ablation of copper based alloys by single and double pulse laser induced breakdown spectroscopy, Appl. Phys. A 85 (2006) 151–157.
[8] L. St-Onge, V. Detalle, M. Sabsabi, Enhanced laser-induced breakdown spectroscopy using the combination of fourth-harmonic and fundamental Nd:YAG laser pulses, Spectrochim. Acta Part B 57 (2002) 121–135.
[9] D.N. Stratis, K.L. Eland, S.M. Angel, Effect of pulse delay time on a pre-ablation dual-pulse LIBS plasma, Appl. Spectrosc. 55 (2001) 1297–1303.
[10] R. Sattmann, V. Sturm, R. Noll, Laser-induced breakdown spectroscopy of steel samples using multiple Q-switch Nd:YAG laser pulses, J.Phys. D 28 (1995) 2181–2187.
[11] C. Gautier, P. Fichet, D. Menut, J.L. Lacour, D. L'Hermite, J. Dubessy, Main parameters influencing the double-pulse laser-induced breakdown spectroscopy in the collinear beam geometry, Spectrochim. Acta Part B 60 (2005) 792–804.
[12] P.A. Benedetti, G. Cristoforetti, S. Legnaioli, A. Salvetti, V. Palleschi, L. Pardini, E. Tognoni, Effect of laser pulse energies in laser induced breakdown spectroscopy in double-pulse configuration, Spectrochim. Acta Part B 60 (2005) 1392–1401.
[13] C. Gautier, P. Fichet, D. Menut, J. Debussy, Applications of the double-pulse laser-induced breakdown spectroscopy (LIBS) in the collinear beam geometry to the elemental analysis of different materials, Spectrochim. Acta Part B 61 (2006) 210–219.
[14] H.W. Bergmann, Excimer laser induced surface modifications and matter interaction using double-pulse-technique (DPT), Appl. Surf. Sci. 96–98 (1996) 287–295.
[15] M. Corsi, G. Cristoforetti, M. Giuffrida, M. Hidalgo, S. Legnaioli, A. Salvetti, V. Palleschi, E. Tognoni, C. Vallebona, Three-dimensional analysis of laser induced plasmas in single and double pulse configuration, Spectrochim. Acta Part B, 59 (2004) 723–735.
[16] L. St-Onge, M. Sabsabi, P. Cielo, Analysis of solids using laser-induced plasma spectroscopy in double-pulse mode, Spectrochim. Acta Part B 53 (1998) 407–415.
[17] F. Colao, V. Lazic, R. Fantoni, S. Pershin, A comparison of single pulse and double pulse laser-induced breakdown spectroscopy of aluminum samples, Spectrochim. Acta Part B 57 (2002) 1167–1179.
[18] C. Gautier, P. Fichet, D. Menut, J.L. Lacour, D. L'Hermite, J. Dubessy, Quantification of the intensity enhancements for the double-pulse laser-induced breakdown spectroscopy in the orthogonal beam geometry, Spectrochim. Acta Part B 60 (2005) 265–276.
[19] G. Cristoforetti, S. Legnaioli, A. Salvetti, V. Palleschi, E. Tognoni, Influence of ambient gas pressure on the laser-induced breakdown spectroscopy technique in the parallel double-pulse configuration, Spectrochim. Acta Part B 59 (2004) 1907–1917.
[20] M. Corsi, G. Cristoforetti, M. Hidalgo, S. Legnaioli, V. Palleschi, A. Salvetti, E. Tognoni, C. Vallebona, Double pulse calibration-free laser-induced breakdown spectroscopy: a new technique for in situ standard-less analysis of polluted soils, Appl. Geochem. 21 (2006) 748–755.
[21] D.N. Stratis, K.L. Eland, S.M. Angel, Dual-pulse LIBS using a pre-ablation spark for enhanced ablation and emission, Appl. Spectrosc. 54 (2000) 1270–1274.

[22] A.M. Prokhorov, V.I. Konov, I. Ursu, I.N. Mihailescu, Laser Heating of Metals, Adam Hilger, Bristol, 1990.
[23] V.N. Tokarev, A.F.H. Kaplan, Suppression of melt flows in laser ablation: application to clean laser processing, J. Phys. D: Appl. Phys. 32 (1999) 1526–1538.
[24] J. Ashkenazy, R. Kipper, M. Caner, Spectroscopic measurements of electron density of capillary plasma based on Stark broadening of hydrogen lines, Phys. Rev. A 43 (1991) 5568–5574.
[25] H.R. Griem, Spectral Line Broadening by Plasmas, Academic Press, New York, 1974.
[26] S. Yalcin, D.R. Crosley, G.P. Smith, G.W. Faris, Influence of ambient conditions on the laser air spark, Appl. Phys. B 68 (1999) 121–130.
[27] H. Klocke, Untersuchungen zum materialabbau durch laserstrahlung, Spectrochim. Acta Part B 24 (1969) 263–281.
[28] C. Geertsen, A. Briand, F. Chartier, J.L. Lacour, P. Mauchien, S. Sjostrom, Comparison between infrared and ultraviolet laser ablation at atmospheric pressure — implications for solid sampling inductively coupled plasma spectroscopy, J. Anal. At. Spectrom. 9 (1994) 17–22.
[29] L.M. Cabalin, J.J. Laserna, Experimental determination of laser induced breakdown thresholds of metals under nanosecond Q-switched laser operation, Spectrochim. Acta Part B 53 (1998) 723–730.
[30] Bleiner, Z. Chen, D. Autrique, A. Bogaerts, Role of laser-induced melting and vaporization of metals during ICP-MS and LIBS analysis, investigated with computer simulations and experiments, J. Anal. At. Spectrom. 21 (2006) 910–921.
[31] Y. Iida, Effects of atmosphere on laser vaporization and excitation processes of solid samples, Spectrochim. Acta Part B 45 (1990) 1353–1367.
[32] D. Bleiner, A. Bogaerts, Multiplicity and contiguity of ablation mechanisms in laser-assisted analytical micro-sampling, Spectrochim. Acta Part B 61 (2006) 421–432.
[33] X. Mao, X. Zeng, S.B. Wen, R.E. Russo, Time-resolved plasma properties for double pulse laser-induced breakdown spectroscopy of silicon, Spectrochim. Acta Part B 60 (2005) 960–967.
[34] J.H. Yoo, S.H. Jeong, R.E. Russo, Explosive change in crater properties during high power nanosecond laser ablation of silicon, J. Appl. Phys. 88 (2000) 1638–1649.
[35] J.H. Yoo, O.V. Borisov, X. Mao, R.E. Russo, Existence of phase-explosion during laser ablation and its effects on Inductively Coupled Plasma-Mass Spectroscopy, Anal. Chem. 73 (2001) 2288–2293.
[36] N.M. Bulgakova, A.V. Bulgakov, Pulsed laser ablation of solids: transition from normal vaporization to phase explosion, Appl. Phys. A 73 (2001) 199–208.
[37] A. Miotello, R. Kelly, Laser-induced phase explosion: new physical problems when a condensed phase approaches the thermodynamic critical temperature, Appl. Phys. A 69 (1999) S67–S73.
[38] M.M. Martynyuk, Critical point parameters of metals, Russ. J. Phys. Chem. 57 (1983) 810–821.
[39] R. Kelly, A. Miotello, Comments on explosive mechanisms of laser sputtering, Appl. Surf. Sci. 96–98 (1996) 205–215.
[40] S. Basu, T. Debroy, Liquid metal expulsion during laser irradiation, J. Appl. Phys. 72 (1992) 3317–3322.